Published by The College of Science & Information Technology (COSIT), TASUED, Vol. 18, No. 1, pp. 39-48.

COSIT, TASUED
Journal of Science and Information Technology (JOSIT)

Free convective magnetohydrodynamic flow of Bingham fluid amid vertical parallel porous plates with viscous and induced magnetic dissipation

***[1]Lawal, O.W., [1]Asade, R.M. and [2]Sikiru. A.B.**

[1]Department Mathematics, Tai Solarin University of Education, Ijagun, Ogun State, Nigeria
[2]Department of Physical, Mathematical and Computer Science, Aletheia University, Ago-Iwoye, Ogun State, Nigeria
**Corresponding Author: waheedlawal207@yahoo.com*

Abstract

The constant two-dimensional magnetohydromagnetic (MHD) free convective flow of an incompressible viscous Bingham fluid, which conducts electricity between two parallel vertical porous plates, has been looked at in the present study. The impact of an induced magnetic field caused by the velocity of an electrically conducting fluid is taken into account. A collection of simultaneous ordinary differential equations govern the motion of the fluid. By employing the perturbation approach, their dimensionless analytical solutions for the temperature field, the induced magnetic field, and the velocity field have been produced. Additionally, the expression for the induced current density was found and computed. The temperature profile, induced current density profile, induced magnetic field profile, and velocity profile are graphically illustrated as a function of several non-dimensional factors. It is discovered that the suction parameter increases the induced magnetic field but decreases the velocity field and induced current density.

Keywords: Porous plates, free convective flow, induced magnetic field, induced current density, viscous and magnetic dissipation

INTRODUCTION

MHD free convective fluxes of viscoplastic fluids, such Bingham fluids, are fundamental to many engineering fields, like chemistry, geophysical, and materials processing. It is essential to comprehend how these intricate fluids behave when subjected to an external magnetic field in order to maximize industrial efficiency.

The MHD free convection flow of a Bingham fluid refers to the study of fluid flow that involves the combined effects of MHD (the study of the magnetic properties of electrically conducting fluids) and free convection (natural fluid motion due to buoyancy forces). The fluid under study in this instance is a Bingham fluid, a kind of non-Newtonian fluid with yield stress, which means that up until a specific stress threshold is crossed, it acts like a solid. Researchers usually take into account the interactions between buoyancy forces, magnetic fields, and the rheological characteristics of the Bingham fluid when examining the MHD free convection flow of a Bingham fluid. The Lorentz force, which results from the interaction between the magnetic field and the electrically conducting fluid, can greatly affect the flow behaviour of the Bingham fluid in the presence of a magnetic field.

In order to account for the unique rheological characteristic of Bingham fluid, the researcher examining this kind of flow frequently with the governing differential equations that define the conservation of momentum, mass, energy, and magnetic inductions. In addition, boundary conditions, material characteristics, and outside variables like temperature gradients and magnetic field intensities might be taken into consideration.

Applications for studying MHD free convection flow of Bingham fluids can be

Cite as:
Lawal, O.W., Asade, R.M. and Sikiru. A.B. (2024). Free convective magnetohydrodynamic flow of Bingham fluid amid vertical parallel porous plates with viscous and induced magnetic dissipation, *Journal of Science and Information Technology (JOSIT)*, Vol. 18, No. 1, pp. 39-48.

found in chemical engineering, materials processing, geophysics, and metallurgy, among other domains. In non-Newtonian fluids, the relationship between shear stress and shear rate is different. There may even be a time-dependent viscosity in the fluid itself. Consequently, it is impossible to define a constant coefficient of viscosity. While viscosity is a widely used term in fluid mechanics to describe a fluid's shear characteristics, it may not be sufficient to characterize non-Newtonian fluids. Employing multiple other rheological properties—which are evaluated using various devices called rheometers and link stress and strain rate tensors under a variety of flow conditions, such as oscillatory shear or extensional flow—is the most efficient way to examine them. Continuum mechanics makes extensive use of tensor-valued constitutive equations, which facilitate a more in-depth examination of the properties. Free convection in vertical channels has been extensively studied under various physical effects in the last few decades due to its significance in numerous engineering applications, such as the temperature control of electronic equipment, the design of passive solar systems for energy conversion, the cooling of nuclear reactors, the design of heat exchangers, chemical devices and process equipment, geothermal systems, and others.

Mohammad-Reza (2015) conducted research on the investigation of entropy formation and heat transport in Bingham plastic fluids within circular microchannels. Their goal is to assess the gap between the two analytical solutions for theoretical assessments of grouting in rock cracks and to theoretically and numerically clarify the form of the plug flow region in the 2D radial flow of a Bingham fluid.

The Phenomenological Friction Equation for turbulent flow of Bingham fluids was explored by Anbarlooei et al. (2017). Under conditions of homogeneous wall heat flux, the thermal properties of Bingham plastic fluid flows are examined in circular micro-channels. Furthermore, according to Zou et al. (2018), grouting is essentially a two-phase flow process where groundwater is displaced in rock fissures by non-Newtonian fluids called grouts. It is therefore always reasonable to expect a certain degree of uncertainty when applying the analytical solutions covered in this book to the operation and design of real systems.

The development of numerical tools for more realistic grout rheological properties in realistic structures of rock fractures and associated networks, as well as for the two-phase flow process, will be a significant step toward the development of quantitative tools for the design and management of rock grouting applications (Zou et al., 2019). Lawal and Erinle (2019) study the viscous dissipation-induced magnetic field-induced MHD flow of a third-grade fluid in a porous channel. They discovered that a higher magnetic field raised the generated magnetic field while decreasing the fluid's velocity. The mathematical analysis of the EMHD laminar flow of Bingham fluid streaming between two Riga plates that created the heat radiation effect was presented by Mollah (2019). He was able to illustrate how various factors, such as the local Nusselt number, affected the flow pattern and the local shear stress using tables and graphs.

In this study, we have taken into account the induced magnetic field while studying the hydromagnetic free convective flow of an electrically conducting, viscous, incompressible Bingham fluid between two parallel vertical porous plates. Using the perturbation technique, the governing equations for the temperature, induced magnetic, and velocity fields have been analytically solved. Additionally, the formula for the induced current density has been obtained. The graphs illustrate how different factors affect the profiles of velocity, induced magnetic field, temperature, and induced current density.

FORMULATION OF THE PROBLEM

We examine the free convective flow under continuous suction between two infinitely vertical porous plates of a viscous incompressible Bingham fluid that conducts electricity. As seen in Figure 1, the x' - axis is perpendicular to the plates and the y' - axis is taken vertically upward along them. There is an h-interval between the plates. While maintaining a steady temperature T_0' on the other plate, one plate is kept at a constant heat

flux. The variables describing the flow will solely rely on the transverse coordinate y' because of the plates infinite area resulting in a single non-zero component in the x' direction of the fluid velocity. A consistent magnetic field $\overline{B}$ of strength B_0 is applied to the plates perpendicularly. The plate at $y'=0$ is thought to be non-conductive, whereas the opposite plate at $y'=h$ is assumed to have electrical conductivity. For a fluid having a high degree of electrical conductivity σ, this in turn induces a magnetic field $\overline{B}$ along the x'- axis. Suppose $q=(u,0,0)$ is the fluid velocity along x'- axis and $\overline{B}=(B_{x,}B_{y,}0)$ is the magnetic field of the system under consideration.

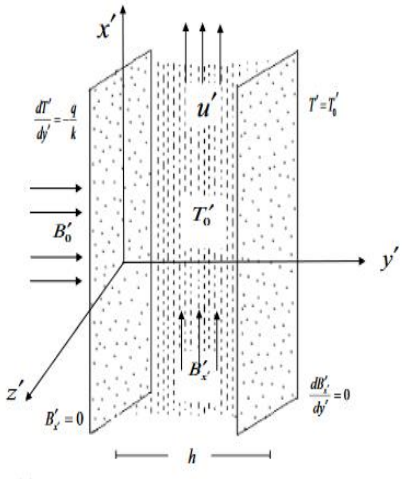

Figure 1. A Schematic diagram of the physical mode

The following is the governing equation of the Bingham fluid when there is an induced magnetic field present but no body forces or body couplings present:

Continuity equation

$$\nabla \cdot q = 0 \tag{1}$$

Momentum equation

$$\rho[(q\cdot\nabla)q] = -\nabla p + \nabla\tau + \mu_{en}\left[(\overline{B}\cdot\nabla)\overline{B}\,\frac{1}{2}\nabla\overline{B}^{2}\right] + \overline{F}_b \tag{2}$$

Energy equation

$$\rho C_p[(q\cdot\nabla)T] = K\nabla^2 T + tr(\tau\cdot l) - \nabla q_r \tag{3}$$

Magnetic induction equation

$$[(q\cdot\nabla)\overline{B}] = (\nabla\cdot\overline{B})q + \frac{1}{\sigma\mu}\nabla^2\overline{B} \tag{4}$$

where $\tau = \mu\dfrac{du}{dy} + \tau_0$ is the stress tensor, ∇ is the operator, ρ is the density of the fluid, $q = u_i + v_j + w_k$ is the velocity of the fluid, C_p is the specific heat capacity of the fluid, K is the thermal conductivity and $\overline{F}_b$ is the buoyancy force which is define as g $\beta(T - T_o)$. With the boundary condition,

$$\begin{aligned} &y=0: u=0,\ \ B_x=0,\ \ \nabla T = -\frac{q_r}{K} \\ &y=h:\ u=0,\ \ \nabla B_x=0,\ \ T=T_0 \end{aligned} \tag{5}$$

METHOD OF SOLUTION

Due to assumption mention earlier, equation (1) to (5) becomes

$$-\frac{dP}{dx} + \mu\frac{d^2u}{dy^2} + \mu_{em}B_0\frac{dB_x}{dy} + g\beta(T-T_0) + v_0\frac{du}{dy} = 0 \tag{6}$$

$$K\frac{d^2T}{dy^2} + v_9\frac{dT}{dy} + \mu\left(\frac{du}{dy}\right)^2 + \tau_0\frac{du}{dy} + \frac{1}{\sigma}\left(\frac{dB_x}{dy}\right)^2 = 0 \tag{7}$$

$$\frac{1}{\sigma\mu}\frac{d^2B_x}{dy^2} + B_0\frac{du}{dy} + v_0\frac{dB_x}{dy} = 0 \tag{8}$$

$$\begin{aligned} &y=0: u=0,\ \ B_x=0,\ \ \frac{dT}{dy} = -\frac{q_r}{K} \\ &y=h:\ u=0,\ \ \frac{dB}{dy}=0,\quad T=T_0 \end{aligned} \tag{9}$$

Introducing the non-dimensional parameters that follow:

$$y=\frac{\bar{y}}{h},\quad q=u=\frac{\mu\bar{u}}{g\beta h^2\nabla\bar{T}}$$

$$B=\frac{\mu}{g\beta h^2\nabla\bar{T}}\sqrt{\frac{\mu_{em}}{\rho}}B_x,\ T=\frac{\bar{T}-\bar{T}_0}{\nabla\bar{T}},$$

$$\nabla T=\frac{hq}{K},\ \Pr=\frac{\mu Cp}{K},\ Pm=\mu\sigma\mu_{em},$$

$$M=\frac{B_0h}{\mu}\sqrt{\frac{\mu_{em}}{\rho}},\ S=\frac{v_0h}{\mu},\ G_r=\frac{vg\beta\nabla T}{v_0^2},$$

$$\alpha=\frac{dP}{dx}$$

equation (6) to (9) in non-dimensional form becomes

$$-\alpha+\frac{d^2u}{dy^2}+S\frac{du}{dy}+M\frac{dB}{dy}+GrT=0 \quad (10)$$

$$\frac{d^2T}{dy^2}+\Pr\frac{dT}{dy}+E_c\Pr\left[\left(\frac{du}{dy}\right)^2+\tau_D\frac{du}{dy}\right] \quad (11)$$
$$+\frac{E_c\Pr}{\Pr m}\left(\frac{dB}{dy}\right)^2=0$$

$$\frac{d^2B}{dy^2}+M\Pr m\frac{du}{dy}+\Pr m\frac{dB}{dy}=0 \quad (12)$$

$$y=0:\ u=0,\ B=0,\ \frac{dT}{dy}=-1$$
$$y=1:\ u=0,\ \frac{dB}{dy}=0,\quad T=0 \quad (13)$$

Now, in order to solve the equations (10) - (12) with boundary conditions given by (13), we apply the perturbation technique

$$\begin{aligned}B(y)&=B_0(y)+E_cB_1(y)+O\left(E_c^2\right)\\ u(y)&=u_0(y)+E_cu_1(y)+O\left(E_c^2\right)\\ T(y)&=T_0(y)+E_cT_1(y)+O\left(E_c^2\right)\end{aligned} \quad (14)$$

Equating the coefficients of the same terms of degree and ignoring terms of $O\left(E_c^2\right)$ after substituting (14) in equations (10) through (13) yields the following ordinary differential equations with their corresponding boundary conditions:

$$-\alpha+\frac{d^2u_0}{dy^2}+S\frac{du_0}{dy}+M\frac{dB_0}{dy}+GrT_0=0 \quad (15)$$

$$u_0=0 \text{ at } y=0 \text{ and } u_0=0 \text{ at } y=1 \quad (16)$$

$$\frac{d^2u_1}{dy^2}+S\frac{du_1}{dy}+M\frac{dB_1}{dy}+GrT_1=0 \quad (17)$$

$$u_1=0 \text{ at } y=0 \text{ and } u_1=0 \text{ at } y=1 \quad (18)$$

$$\frac{d^2u_2}{dy^2}+S\frac{du_2}{dy}+M\frac{dB_2}{dy}+GrT_2=0 \quad (20)$$

$$\frac{d^2T_0}{dy^2}+\Pr\frac{dT_0}{dy}=0 \quad (21)$$

$$\frac{dT_0}{dy}=-1 \text{ at } y=0$$
$$\text{and } T_0=0 \text{ at } y=1 \quad (22)$$

$$\frac{d^2T_1}{dy^2}+\Pr\frac{dT_1}{dy}+\Pr\left[\left(\frac{du_0}{dy}\right)^2+\tau_D\frac{du_0}{dy}\right] \quad (23)$$
$$+\frac{\Pr}{\Pr m}\left(\frac{dB_0}{dy}\right)^2=0$$

$$\frac{dT_1}{dy}=0 \text{ at } y=0 \text{ and } T_1=0 \text{ at } y=1 \quad (24)$$

$$\frac{d^2T_2}{dy^2}+\Pr\frac{dT_2}{dy}+2\Pr\frac{du_0}{dy}\frac{du_1}{dy}+\Pr\tau_D\frac{du_1}{dy}$$
$$+\frac{2\Pr}{\Pr m}\frac{dB_0}{dy}\frac{dB_1}{dy}=0 \quad (25)$$

$$\frac{dT_2}{dy}=0 \text{ at } y=0 \text{ and } T_2=0 \text{ at } y=1 \quad (26)$$

$$\frac{d^2B_0}{dy^2}=0 \quad (27)$$

$$B_0=0 \text{ at } y=0$$
$$\text{and } \frac{dB_0}{dy}=0 \text{ at } y=1 \quad (28)$$

$$\frac{d^2B_1}{dy^2}+M\Pr m\frac{du_0}{dy}+\Pr m\frac{dB_0}{dy}=0 \quad (29)$$

$$B_1=0 \text{ at } y=0$$

and $\frac{dB_1}{dy} = 0 \quad \text{at} \quad y = 1$ (30)

$$\frac{d^2 B_2}{dy^2} + M \,\mathrm{Pr}\, m \frac{du_1}{dy} + \mathrm{Pr}\, m \frac{dB_1}{dy} = 0 \tag{31}$$

$B_2 = 0$ at $y = 0$

and $\frac{dB_2}{dy} = 0$ at $y = 1$ (32)

The solution of (27) under the transformed boundary conditions given by (28) yield

$$B_0 = 0 \tag{33}$$

Similarly, the solution of (21) under the transformed boundary conditions given by (22) yield

$$T_0 = a_1 + \frac{e^{-\mathrm{Pr}\, y}}{\mathrm{Pr}} \tag{34}$$

Substituting equation (33) and (34) into equation (15) and solve with boundary condition (16) to obtain

$$u_0 = a_9 e^{-Sy} - a_{10} e^{-\mathrm{Pr}\, y} + a_6 y + a_7 \tag{35}$$

Equation (33) and (35) were substitute into equation (29) and compute with boundary condition (30) to yield

$$B_1 = a_{11} e^{-Sy} - a_{12} e^{-\mathrm{Pr}\, y} - a_{13} y^2 + a_{14} y - a_{15} \tag{36}$$

Substituting equation (35) and (33) into equation (23) and solve with boundary condition (24) to obtain

$$T_1 = a_{24} e^{-2Sy} a_{23} e^{-\mathrm{Pr}\, y - Sy} - a_{22} e^{-Sy} - a_{20} e^{-\mathrm{Pr}\, y} + a_{21} e^{-2\,\mathrm{Pr}\, y} + a_{19} e^{-\mathrm{Pr}\, y} y + a_{18} y - a_{16} \tag{37}$$

Also, Equation (36) and (37) were substitute into equation (17) and compute with boundary condition (18) to gives

$$u_1 = a_{38} e^{-2Sy} + (a_{34} + a_{35} y + a_{36} + a_{37} e^{-\mathrm{Pr}\, y}) e^{-Sy} + a_{33} e^{-\mathrm{Pr}\, y} + (a_{31} y + a_{32}) e^{-\mathrm{Pr}\, y} + a_{30} y^2 + a_{29} y - a_{26} \tag{38}$$

The induced current density is given as

$$J = -\frac{dB}{dy} = \frac{a_7 S}{e^{Sy}} - \frac{a_8 \,\mathrm{Pr}}{e^{\mathrm{Pr}\, y}} + 2a_9 y + a_{10} \tag{39}$$

The skin friction is the other physical quantity of interest, as we now know how the velocity is expressed. Consequently, the non-dimensional skin friction values on both walls are provided.

(40)

$$\tau_0 = \left(\frac{du}{dy}\right)_{y=0} = a_4 + \frac{-a_1 S e^{-Sy} - a_2 S e^{-Sy} + a_3 \,\mathrm{Pr}\, e^{-\mathrm{Pr}\, y}}{a_6} + 2a_{33} y + a_{34} + \frac{a_{36}}{e^{\mathrm{Pr}\, y}} - \frac{a_{36} y \,\mathrm{Pr}}{e^{\mathrm{Pr}\, y}} - \frac{a_{35} \,\mathrm{Pr}}{e^{\mathrm{Pr}\, y}} - \frac{2a_{37} \,\mathrm{Pr}}{\left(e^{\mathrm{Pr}\, y}\right)^2} - \frac{a_{38} S}{e^{Sy}} - \frac{a_{39}}{e^{Sy}} - \frac{a_{39} y S}{e^{Sy}} - \frac{a_{39} \,\mathrm{Pr}}{a_{32} e^{\mathrm{Pr}\, y} e^{Sy}} - \frac{a_{29} S}{a_{32} e^{\mathrm{Pr}\, y} e^{Sy}} - \frac{2a_{40} S}{\left(e^{Sy}\right)^2}$$

(41)

$$\tau_1 = \left(\frac{du}{dy}\right)_{y=1} = -a_4 + \frac{-a_1 S e^{-Sy} - a_2 S e^{-Sy} + a_3 \,\mathrm{Pr}\, e^{-\mathrm{Pr}\, y}}{a_6} + 2a_{33} y + a_{34} + \frac{a_{36}}{e^{\mathrm{Pr}\, y}} - \frac{a_{36} y \,\mathrm{Pr}}{e^{\mathrm{Pr}\, y}} - \frac{a_{35} \,\mathrm{Pr}}{e^{\mathrm{Pr}\, y}} - \frac{2a_{37} \,\mathrm{Pr}}{\left(e^{\mathrm{Pr}\, y}\right)^2} - \frac{a_{38} S}{e^{Sy}} - \frac{a_{39}}{e^{Sy}} - \frac{a_{39} y S}{e^{Sy}} - \frac{a_{39} \,\mathrm{Pr}}{a_{32} e^{\mathrm{Pr}\, y} e^{Sy}} - \frac{a_{29} S}{a_{32} e^{\mathrm{Pr}\, y} e^{Sy}} - \frac{2a_{40} S}{\left(e^{Sy}\right)^2}$$

where $a_1, a_2, a_3, \ldots\ldots, a_{40}$ used in the equation are constant.

RESULTS AND DISCUSSION

Several physical parameters, including the suction parameter (*S*), the magnetic Prandtl number (*Prm*), the Hartmann number (*M*), and the Prandtl number (Pr) characterize the current MHD free convection model of Bingham fluid with induced magnetic field. The diagrams illustrate how different parameters affect the velocity profile, induced magnetic field profile, and induced current density profile. The Prandtl number (*Pr*) and the suction parameter(*S*) are the sole factors that alter the temperature distribution; the graphs also display how these parameters affect the temperature profiles.

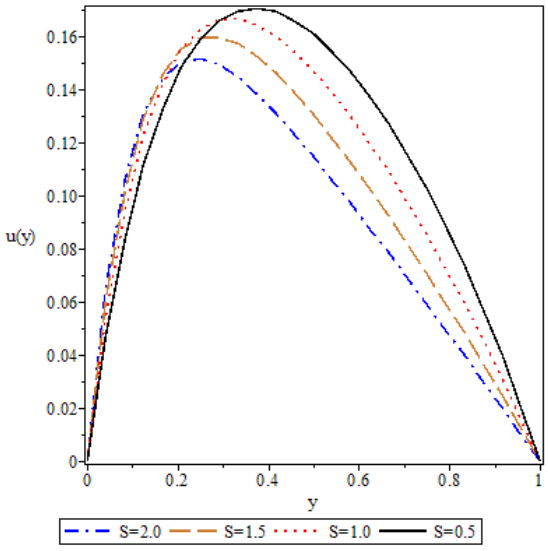

Figure 2. Effect of Suction parameter S on velocity profile when $\alpha = 2, \Pr = 0.7,$ $\Pr m = 0.5, Gr = 5.0, M = 5$

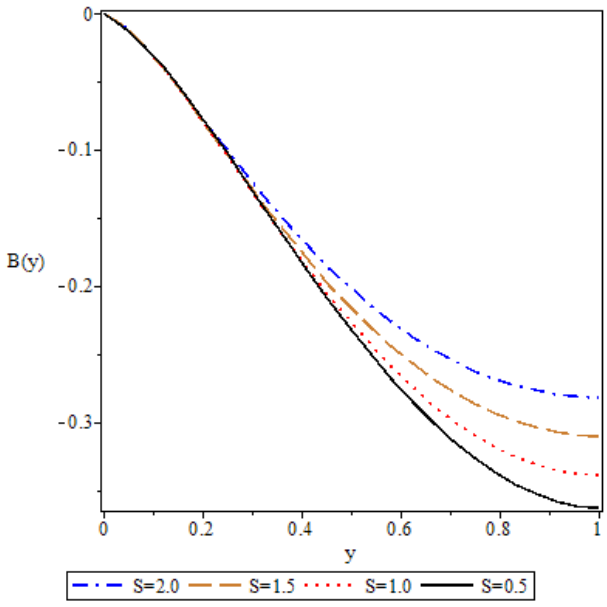

Figure 3. Effect of Suction parameter S on induced magnetic field $\alpha = 2, \Pr = 0.7,$ $\Pr m = 0.5, Gr = 5.0, M = 5$

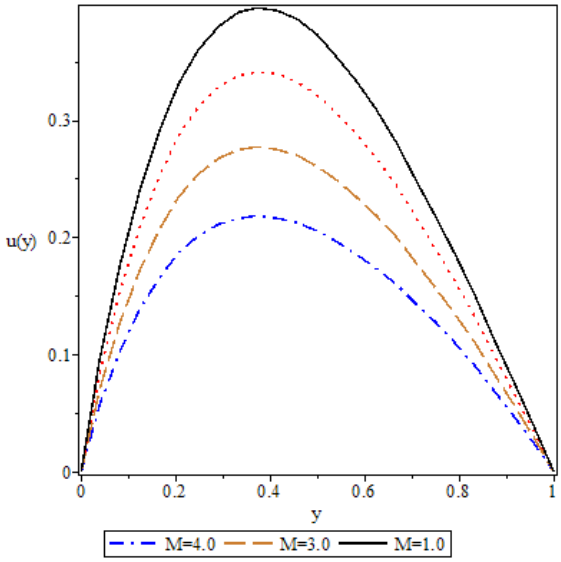

Figure 4. Effect of magnetic parameter M on velocity profile when $\alpha = 2, \Pr = 0.7,$ $\Pr m = 0.5, Gr = 5.0, S = 2.0$

The impact of the suction parameter on the velocity and induced magnetic field profile is depicted in Figures 2 and 3. It is discovered that, as shown in Figure 3, an increase in the suction parameter causes a drop in the velocity profiles as well as an induced magnetic field.

The influence of the magnetic parameter on the velocity and induced magnetic field profile can be seen in Figures 4 and 5. It is discovered that both the induced magnetic profile and velocity decrease with an increase in the magnetic parameter.

Figures 6 and 7 show how the thermal Grashof number affects the velocity and induced magnetic field profile. It has been found that when Grashof number increases, the velocity profile increases but the induced magnetic field values stay negative, indicating a distinct absolute decrease in the induced magnetic field as Gr increases.

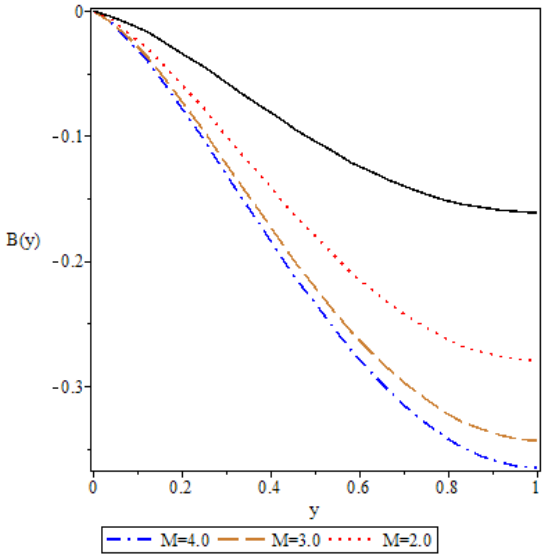

Figure 5. Effect of magnetic parameter M on induced magnetic profile when $\alpha = 2, \Pr = 0.7,$ $\Pr m = 0.5, Gr = 5.0, S = 2.0$

Magnetic Prandtl number affects velocity and induced magnetic field profile, as seen in Figures 8 and 9. A rise in magnetic Prandtl number results in a low velocity and induced magnetic field profile.

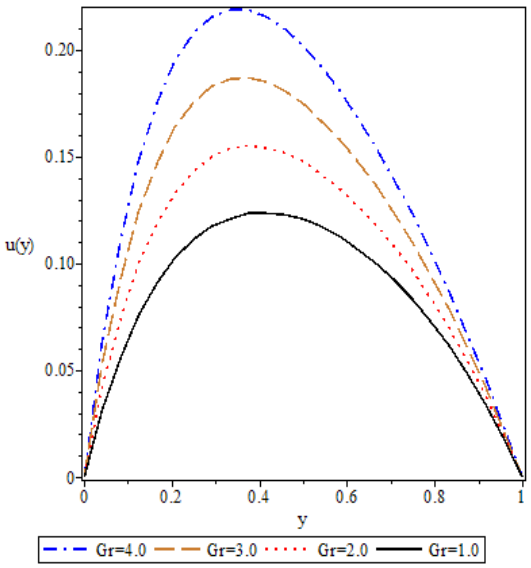

Figure 6. Effect of Grasshof number Gr on velocity profile when $\alpha = 2, \Pr = 0.7,$ $\Pr m = 0.5, M = 5.0, S = 2.0$

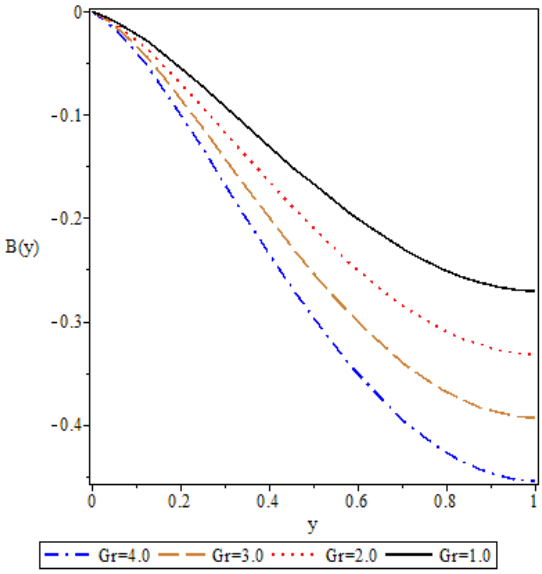

Figure 7. Effect of Grasshof number Gr on induced magnetic field when $\alpha = 2, \Pr = 0.7,$ $\Pr m = 0.5, M = 5.0, S = 2.0$

Figures 10 and 11 depict the fluid velocity profile and induced magnetic field, which both exhibit increasing behavior as the Prandtl number increases. In contrast, Figure 12 displays an initial increase followed by a subsequent decrease in the temperature profile as the Prandtl number increases.

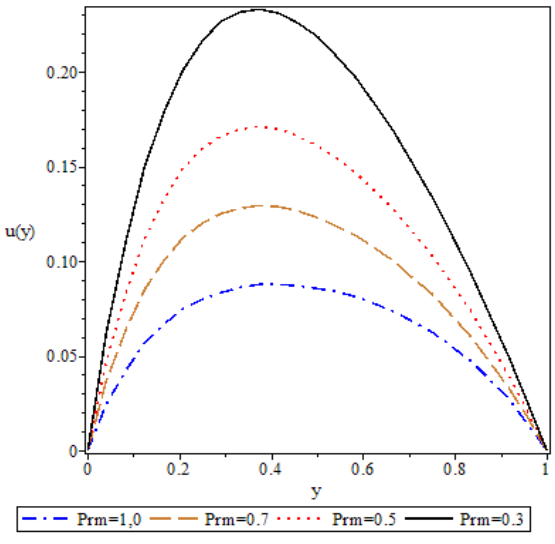

Figure 8. Effect of magnetic Prandtl number $\Pr m$ on velocity profile when $\alpha = 2, \Pr = 0.7,$ $Gr = 0.5, M = 5.0, S = 2.0$

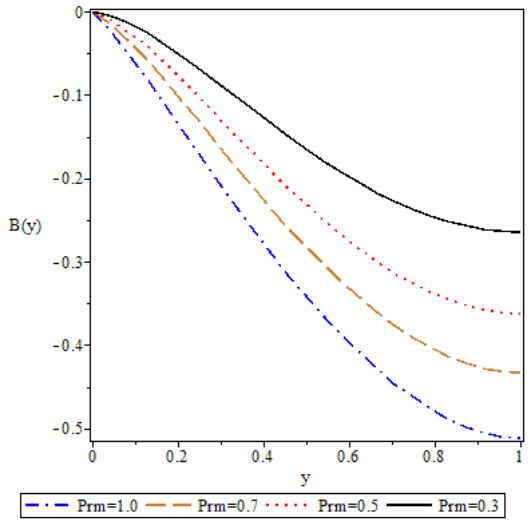

Figure 9. Effect of magnetic Prandtl number $\Pr m$ on induced magnetic profile when $\alpha = 2, \Pr = 0.7,$ $Gr = 0.5, M = 5.0, S = 2.0$

Figure 13 illustrates how the induced current density varies with the magnetic Prandtl number *Prm*, and Figure 14 shows how it varies with the Hartmann number *M*. The figures make it evident that there is a rising trend in the impact of the magnetic Prandtl number and the Hartmann number on the induced current density profile. As the Prandtl number *Pr* increases, the induced current density falls, as Figure 15 illustrates.

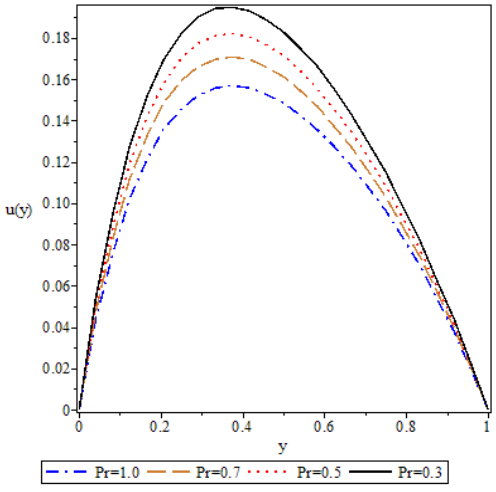

Figure 10. Effect of Prandtl number $\Pr$ on the velocity profile when $\alpha = 2, \Pr m = 0.5,$ $Gr = 0.5, M = 5.0, S = 2.0$

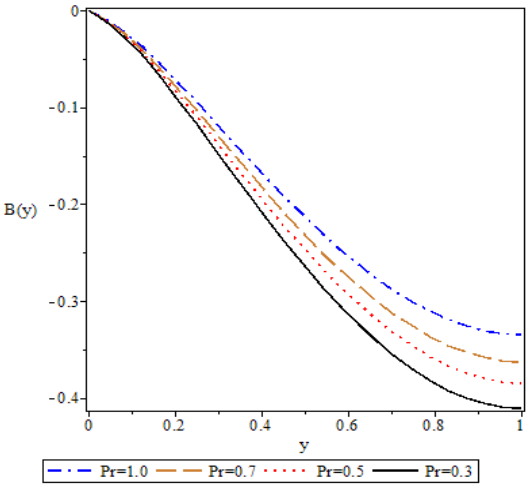

Figure 11. Effect of Prandtl number $\Pr$ on the velocity profile when $\alpha = 2, \Pr m = 0.5,$ $Gr = 0.5, M = 5.0, S = 2.0$

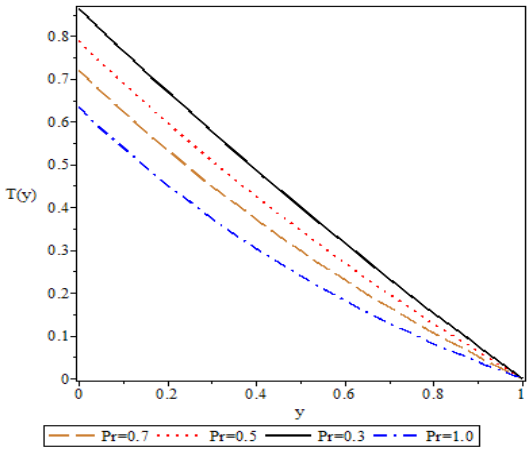

Figure 12. Effect of Prandtl number $\Pr$ on the temperature profile when $\alpha = 2, \Pr m = 0.5,$ $Gr = 0.5, M = 5.0, S = 2.0$

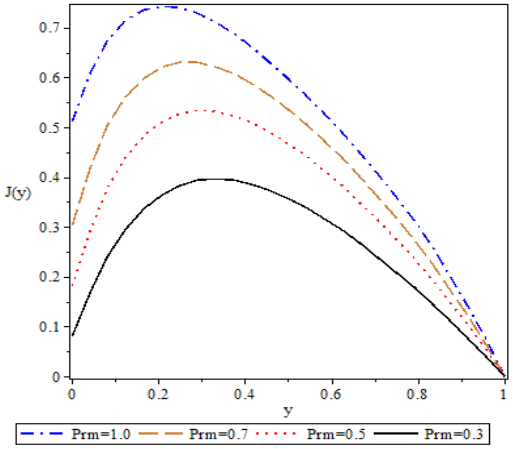

Figure 13. Effect of magnetic Prandtl number $\Pr m$ on induced current density when $\alpha = 2, \Pr = 0.7,$ $Gr = 0.5, M = 5.0, S = 2.0$

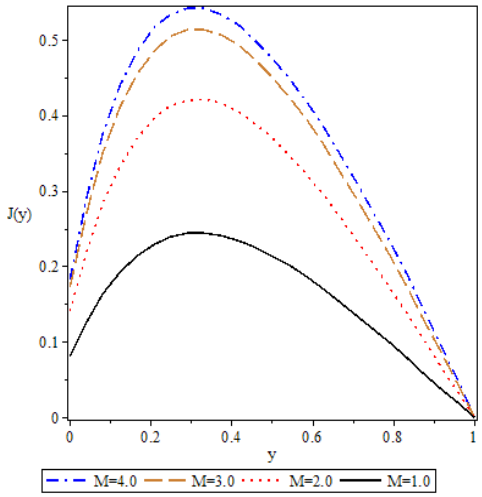

Figure 14. Effect of magnetic parameter M on Induced current density when $\alpha = 2, \Pr = 0.7, \Pr m = 0.5, Gr = 5.0, S = 2.0$

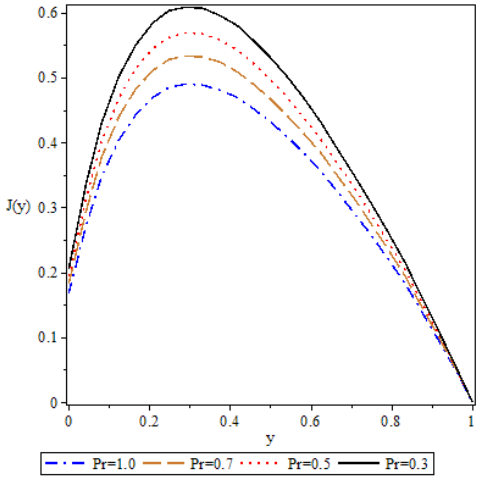

Figure 15. Effect of Prandtl number $\Pr$ on the Induced current density when $\alpha = 2, \Pr m = 0.5, Gr = 0.5, M = 5.0, S = 2.0$

Table 1. Suction velocity and magnetic Prandtl number effects on skin friction

S	$\alpha = 2, \Pr = 0.7, \Pr m = 0.5, Gr = 5.0, M = 5$		Prm	$\alpha = 2, \Pr = 0.7, Gr = 0.5, M = 5.0, S = 2.0$	
	τ_0	τ_1		τ_0	τ_1
0.5	1.242182	-0.691530	0.3	1.876976	-0.680407
1.0	1.308804	-0.643910	0.5	1.446132	-0.557201
1.5	1.376947	-0.599094	0.7	1.126402	-0.476159
1.0	1.446132	-0.557201	1.0	0.762722	-0.395891

Table 2: Prandtl number and Hartmann effects on skin friction

Pr	$\alpha = 2, \Pr m = 0.5, Gr = 0.5, M = 5.0, S = 2.0$		M	$\alpha = 2, \Pr = 0.7, \Pr m = 0.5, Gr = 5.0, S = 2.0$	
	τ_0	τ_1		τ_0	τ_1
0.3	1.446132	-0.557200	1.0	2.515458	-0.923115
0.5	1.350727	-0.534466	2.0	2.213559	-0.826580
0.7	1.267199	-0.515231	3.0	1.857102	-0.711315
1.0	1.160754	-0.491771	4.0	1.531828	-0.604303

Table 1 displays the effects of the magnetic Prandtl number and the suction parameter on the skin friction on the two plates. This table unequivocally demonstrates that as the suction velocity increases, so does the skin friction on both plates. Additionally, skin friction on one plate reduces at and increases on the other plate at a higher magnetic Prandtl number.

Table 2 illustrates the impact of the Hartmann and Prandtl numbers on skin friction. It is observed that skin friction increases on the plate at y = 1 and reduces on the plate at y = 1 when the values of the Prandtl and Hartmann numbers grow.

CONCLUSION

An analysis has been conducted on the hydromagnetic free convective flow between two vertical parallel porous plates, considering the influence of an induced magnetic field. It is found that the velocity profiles decrease when the suction parameter, Prandtl number, magnetic Prandtl number, and Hartmann number increase. Additionally, it is noted that the induced magnetic field increases with increases in the suction parameter, the Prandtl number, and the Hartmann number, but decreases with increases in the magnetic Prandtl number. When the magnetic Prandtl number rises, the induced current density profile rises as well; however, when the suction parameter, Hartmann number, and Prandtl number rise, it falls.

When creating engineering designs, the suction/injection velocity on the porous plates can be adjusted to control the velocity and induced magnetic field.

REFERENCES

Odelu,O. and Naresh Kumar, N. (2015). Unsteady MHD Flow and Heat Transfer of Micropolar Fluid in a Porous Medium between Parallel plates", *Canadian Journal of Physics*, **93**, 880-887

Ashraf, M. B., Hayat, T., Alsaedi, T. and Shehzad, S. A. (2015). Convective heat and mass transfer in MHD mixed convection flow of Jeffrey nanofluid over a Radially Stretching Surface with Thermal Radiation", *Journal Central South University*, **22**, 1114-23

Anbarlooei, H, R., Cruz, D. O., Ramos, F., Cecilia M. M. S and Silva A. P. (2017). Phenomenological friction equation for turbulent flow of Bingham fluids.Science Direct, 8(2), 184-193

Mohammad-Reza Mohammadi (2015) studied Heat Transfer and Entropy Generation Analysis of Bingham Plastic Fluids in Circular Microchannels. International Journal of Science and Technology. , 9(4), 180-187

Lawal O. W. and Erinle L. M. (2019). An investigative study of the MHD flow of a third grade fluid in a porous channel under the influence of an induced magnetic field with viscous dissipation. Islamic University Multidisciplanary Journal. 6(3), 187-201

Mollah, M. T (2019). EMHD laminar flow of Bingham fluid between two parallel Riga plates. International Journal of Heat and Technology. 37 (2), 641-648